Cohesion and aggregates in unsaturated wet granular flows down a rough incline

Stephanie Deboeuf, Abdoulaye Fall

Cohesion and aggregates in unsaturated wet granular flows down a rough incline

S. Deboeuf[1, a)] and A. Fall[2]
[1)]*Sorbonne Université, CNRS, UMR 7190, Institut Jean Le Rond d'Alembert, F-75005 Paris, France*
[2)]*Laboratoire Navier UMR 8205, CNRS, Ecole des Ponts ParisTech, Univ. Gustave Eiffel, Cité Descartes-Marne-la-Vallée, France*

(Dated: 31 May 2023)

Multi-phase flows, encountered in nature or in industry, exhibit non-trivial rheological properties, that we attempt to better understand thanks to model materials and appropriate rheometers. Unsaturated wet granular flows down a rough inclined plane turn out to be steady and uniform for a wide range of parameters, despite the cohesion and the grain aggregates. The cohesive Mohr-Coulomb yield criterion extended to inertial granular flows, with a cohesion stress dependent on the liquid content and an internal friction coefficient dependent on the inertial number, allows for predictions in good agreement with our experimental measurements, when one introduces a grain aggregate size, which defines the appropriate length and relaxation time scales in the inertial number. We found that the grain aggregate size depends not monotonically on the liquid content and does not scale with the cohesion length induced by the cohesion stress, due to the non-trivial distribution of the liquid within the granular material.

I. INTRODUCTION

Wet granular materials are complex systems with grains, liquid and gas that have cohesion properties and form aggregates. They are found in various natural and industrial processes (landslides, debris flows, rock or snow avalanches, civil engineering, powder-process such as wet granulation, fertilizer production or coating) and their rheology is still not fully understood. Their flow behaviour is influenced by many factors, and experimental instrumentation is challenging. Therefore, a unified approach combining theoretical, numerical and experimental results is needed to better understand their behaviour.

When liquid is added to granular materials, it can create cohesion between the grains due to the surface tension of the liquid, which forms capillary bridges between the grains. This leads to the formation of clusters of grains, also known as grain aggregates [1,2]. Cohesion is in addition to the frictional forces between the particles. To describe this cohesion at a macroscopic level, the cohesive Mohr-Coulomb yield criterion is commonly used in soil mechanics and geomechanics:

$$\tau = \tau_c + \mu_0 P, \tag{1}$$

with τ_c, the cohesion stress and μ_0, the static internal friction coefficient, where τ and P are the shear stress and the normal confining stress (or pressure) respectively.

This successfully describes plastic flows of unsaturated wet grains, in the quasi-static limit of slow flows, with the same static internal friction coefficient μ_0 for wet and dry grains[2–6], that can be interpreted as the absence of modification of the inter-grain friction in the quasi-static limit[7,8], despite the presence of liquid[9,10].

A cohesion length ℓ_c can be defined from the cohesion stress τ_c [11,12] as:

$$\ell_c = \frac{\tau_c}{\rho g}, \tag{2}$$

that allows to predict the maximal height of a stable cohesive granular column[11], as well as the characteristic lengths of the roughness of a deposit after the collapse of an unstable column[12].

What about the case of non-quasi-static, but inertial, flows? The validity of Eq. (1) beyond yield and its extension to inertial cohesive granular flows is still an open question.

The consequences of liquid among grains being not obvious, unsaturated wet granular materials are not as simple as purely cohesive materials, with the addition of a single inter-grain force interaction characterized by a maximum force F_c present at all contacts[9,13,14]. The influence of liquid wetting the grains on the rheology sensitively depends on the liquid content and its spatial distribution around grains i.e. the morphology of the liquid phase[1,15]. Such a mixture of grains, liquid and air may have either a solid-like behaviour[16] or a liquid-like behaviour[17], both being different than the behaviours of dry grains. Their solid-like properties, due to friction and cohesion, enable the building of wet sand castles as opposed to dry sand which cannot stabilize under gravity with slopes steeper than some finite angle[18,19]. Their liquid-like properties are strongly modified by the presence of cohesive inter-grain forces; in particular, the particle velocity and the contribution of particle collisions to the dissipation mechanisms are reduced by the presence of liquid[10,20–23]. Due to the high solid fraction of grains and close distances between bonded grains, direct inter-grain contacts play an important role in the physical mechanisms ruling their rheological behaviour, which is strongly affected by the grain shape, surface and properties (roughness, friction, elasticity, ...). To those micromechanical features, one should add the physical properties of the liquid (viscosity, surface tension, contact angle) and the geometrical microstructural properties[1,15].

Unsaturated wet granular materials are at the crossroads of dry and fully immersed granular materials, about which there is an ample literature based on laboratory rheometric measurements and numerical simulations[8,24–29]. As introduced by Bocquet *et al.* [18], "In 1773 Coulomb [30] recognized that the static properties of granular systems can be discussed in terms of the frictional properties between different layers". Since,

[a)]stephanie.deboeuf@cnrs.fr

the rheology of a granular material either in static configurations or in inertial flows is encoded by the apparent friction μ^{app}:

$$\mu^{app} = \frac{\tau}{P}. \quad (3)$$

The considerable advances in the modeling of dense granular flows [24,25,31,32] have led to the description of the variations of $\mu^{app}(I)$ as a function of the inertial number I:

$$I = \frac{\dot{\gamma} d}{\sqrt{P/\rho}}, \quad (4)$$

with $\dot{\gamma}$ the shear rate, d and ρ, the grain size and density respectively. This constitutive "friction" law was applied successfully to different flow geometries, coupled to the solid volume fraction $\phi(I)$, defined as the ratio of the grain volume over the total volume, which is also related to the inertial number I, and often referred to as the "dilatancy" law. The common interpretation of the I-dependence lies in the comparison of two time scales at the elementary scale level (one grain for dry cohesionless granular materials): the typical time of deformation $1/\dot{\gamma}$ and the free-fall relaxation time $d\sqrt{\rho/P}$, when the ambient fluid does not apply any drag on the grain.

Cohesive granular materials were less studied, but exhibit a much wider variety of internal structures, depending on the assembling procedure [33]. Their internal state and their density are quite sensitive to a second dimensionless number –referred to as either a reduced pressure $P^* = Pd^2/F_c$ [2,34,35] or a cohesion index $1/P^*$ [6,9,36]– comparing the inter-grain cohesive force F_c to the confining one Pd^2 [2,6,13,34,35]. In dense flows, the friction law becomes:

$$\mu^{app}(I, P^*), \quad (5)$$

as well as the dilatancy law: $\phi = \phi(I, P^*)$. Mandal, Nicolas, and Pouliquen [14] recently observed in numerical simulations that the cohesion force F_c should be changed by an effective cohesion force $F_c^{eff}(F_c, k_n, e, d)$ to take into account the effect of the grain stiffness k_n, elasticity e and diameter d.

Recently, based on stress additivity, Vo *et al.* [36] proposed that both numbers should be combined into one single cohesive visco-inertial number which would solely control macroscopic stresses and micromorphologies [6,29]. This cohesive visco-inertial number is equivalent to the inertial number I (4) for dry cohesionless granular media and to some viscous number in the limit of low inertia and cohesion [7,28].

An extension of the cohesive Mohr-Coulomb yield criterion (1) to inertial flows, as done by some authors [2,6,9,11,34,35], simply states that the internal friction coefficient μ and the cohesion stress τ_c are two independent strength properties of the flow. Then the rheology of cohesive granular materials is described by two distinct functions $\mu(I)$ and $\tau_c(I)$ so that:

$$\tau = \tau_c(I) + \mu(I)\, P. \quad (6)$$

But Eq. (6) does not allow to collapse cohesive and cohesionless granular flows, what may require a more general dimensionless number [6,36]. Note that Eq. (6) is consistent with Eq. (5).

It's worth noting that the internal friction coefficient μ and the apparent friction coefficient μ^{app} are different for cohesive materials, while they are the same for cohesionless granular materials. This means that even with the same internal friction coefficient μ for both dry and unsaturated wet grains, the presence of a non-zero cohesion stress τ_c results in a larger apparent friction coefficient μ^{app}, which leads to larger slope angles [16,18].

How do cohesive forces, such as that present in unsaturated wet grains, affect dense granular flows? A standard configuration to study the flow of granular materials is the rough inclined plane. Indeed, the gravity-induced free-surface flow of grains has a number of engineering and geophysical applications. Furthermore, the inclined plane can serve as a rheometer, since regimes of steady uniform flows lead to apparent-friction-controlled experiments [24,37–40]. To our knowledge, among the broad literature about granular flows down a rough inclined plane, no experimental study was dedicated to the case of unsaturated wet materials (or cohesive granular materials in general, which cohesion is of another nature than capillary), while only a few numerical studies were reported [13,14,41]. These numerical works observed i) the emergence of a plug-flow of a finite thickness at the surface, above a sheared region, that is not observed in the case of a cohesionless granular flow, ii) a solid fraction roughly constant in the sheared region, iii) a velocity profile which is not consistent with a Bagnold profile.

In this article, we present an experimental study of the flow of frictional and cohesive (unsaturated wet) grains down a rough inclined plane, when cohesion is induced by a wetting liquid, partially saturating the pores of a granular material. By changing the liquid content, we will compare such free-surface gravitational flows of unsaturated wet grains with those of dry cohesionless materials made up of the same grains, and we will investigate the validity of Eq. (6). Our paper is organized as follows. The experimental setup and the measurement methods are outlined in Section II. The main experimental results with some theoretical predictions for steady uniform shear flows are presented in section III. A conclusion is given in section **??**.

II. EXPERIMENTAL MATERIALS AND METHODS

A. Particles and fluids

Our model granular materials are hard and non-Brownian solid spherical beads, mixed with a non-volatile, wetting, Newtonian liquid. Glass beads of density $\rho = 2500\text{kg m}^{-3}$ and of diameter $d \simeq 250 \pm 50\mu\text{m}$ and silicon oil (47V20) of density $\rho_l = 950\text{kg m}^{-3}$, viscosity $\eta = 20\text{mPa s}$ and surface tension $\Gamma = 20\text{mN m}^{-1}$ are used. Oil is used instead of water to minimize evaporation. The Bond number of our unsaturated wet granular materials, comparing cohesive to gravitational grain scale forces, defined as $Bo = \rho g d^2/\pi\Gamma = 10^{-2} \ll 1$, with g the gravity acceleration, is thus small enough to be in a cohesive regime. Indeed, cohesive forces exerted via capillary bridges and liquid/air clusters on bounded grains (due to difference of pressure between liquid and air and surface tension

in the interfaces) become important compared to their weight if their diameter d is much smaller than the capillary length $\sqrt{\pi\Gamma/\rho g}$.

We always prepare the system in the same way to ensure reproducible experimental conditions: the wetting liquid is mixed thoroughly with dry beads until a uniform consistency is visually obtained. Different liquid contents $\epsilon = m_l/m_s$, defined as the mass ratio of liquid over grains, are used: $\epsilon = 0$ and $\epsilon \in [0.1\%\text{-}1.4\%]$, so that we focus in this work on the dry state and on unsaturated wet samples, these latter being in the pendular or funicular state. Here, we consider that the wet granular material density $\rho(1+\epsilon) \simeq \rho$. In the pendular state, liquid bridges are of small volumes and particles are held together at their contact points (or where they are close to contact) by liquid bridges[1]. By contrast, in the funicular state, some pores are fully saturated by liquid, but there still remains voids filled (partially or not) with air[15], so liquid/air clusters appear and wet grains aggregate.

In the literature, the volume ratio of liquid over grains $w = \epsilon\,\rho/\rho_l \in [0.26\%\text{-}3.7\%]$ or the liquid fraction $\phi_l = \phi\,\rho/\rho_l\,\epsilon \in [0.16\%\text{-}2.2\%]$ defined as the ratio of liquid over total volumes, may be alternatively used. On average, pores are filled with only a small quantity of liquid at $\phi_l/(1-\phi) \in [0.4\%\text{-}5\%]$. The solid fraction ϕ of unsaturated wet grains is reported to be smaller than the one of cohesionless dry materials $\phi(\epsilon = 0) \simeq 60\%$ and to change between 50% and 57%[42–44]. In the following, the solid fraction is taken equal to $\phi \approx 60\%$ for dry grains and for unsaturated wet grains, this assumption having roughly no significant effect on our results, as we have systematically checked.

B. Experimental set-up

The experimental set-up is sketched in Fig. 1(a), its main parts being a hopper, an inclined plane, a LASER diode, a CCD camera, a scale, which roles will be detailed below. A mass of about 20kg of (unsaturated wet or dry) grains is stored into the hopper located at the top of the inclined plane, before opening the hopper frontal gate to release them. The 1.6m-long plane is made of a rough bottom plate and two smooth lateral Plexiglass walls. The rough surface is made of sandpaper of roughness $\simeq 350\mu$m, which is the same order as the grain diameter, to ensure a no-slip boundary condition at the bottom. The width between the side walls is $W = 34\text{cm} = 1360d$, and the range of our control parameters lead to shear flows deep inside the granular layer up to the bottom plate, and not only at the surface like in a heap flow, allowing to neglect sidewall effects[45].

The plane can be inclined at the imposed slope angle θ. The hopper is elevated ($\sim$ 10cm) with respect to the incline, so that when opening its gate, the beads first fall down continuously before flowing down the rough plane. This thin and dilute 'rain' allows a constant input mass flow rate Q_m[46] and a reproducible initial condition.

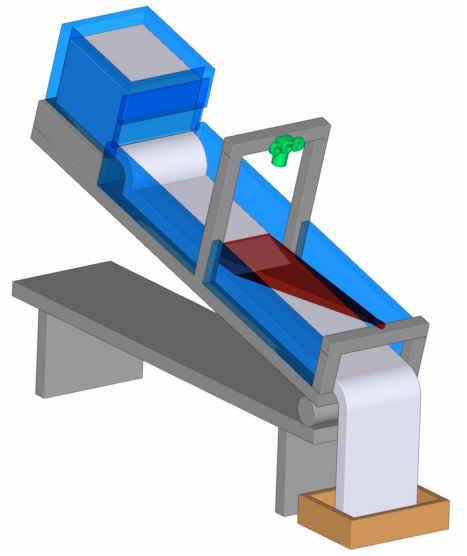

(*a*)

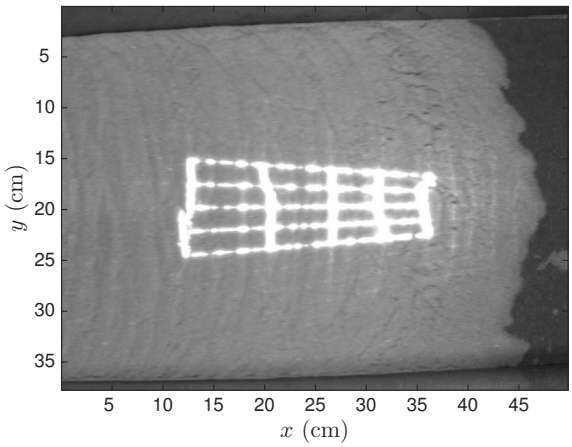

(*b*)

FIG. 1. (*a*) The experimental set-up consists of a rough plane that can be inclined at the imposed slope angle θ. Unsaturated wet or dry grains, stored in a hopper at the top of the plane, are released through a gate, which aperture opening height f can be adjusted in order to control the mass flow rate Q_m, measured by means of a scale located underneath. The granular layer free surface is recorded by a CCD camera. A LASER diode is used to produce a grid sheet for profilometry to measure thickness profiles $h(x,y,t)$. (*b*) A picture of the free surface of a unsaturated wet granular flow on the incline at $\theta = 31°$ and $f = 5$cm.

C. A typical granular flow

For a given granular flow, the two control parameters are the hopper frontal gate opening height f and the inclination angle θ. Both control parameters f and θ affect the mass flow rate (the velocity and the thickness of the flow too), whereas only the slope angle θ controls the apparent friction μ^{app} within the granular layer for steady uniform flows. For too low mass flow

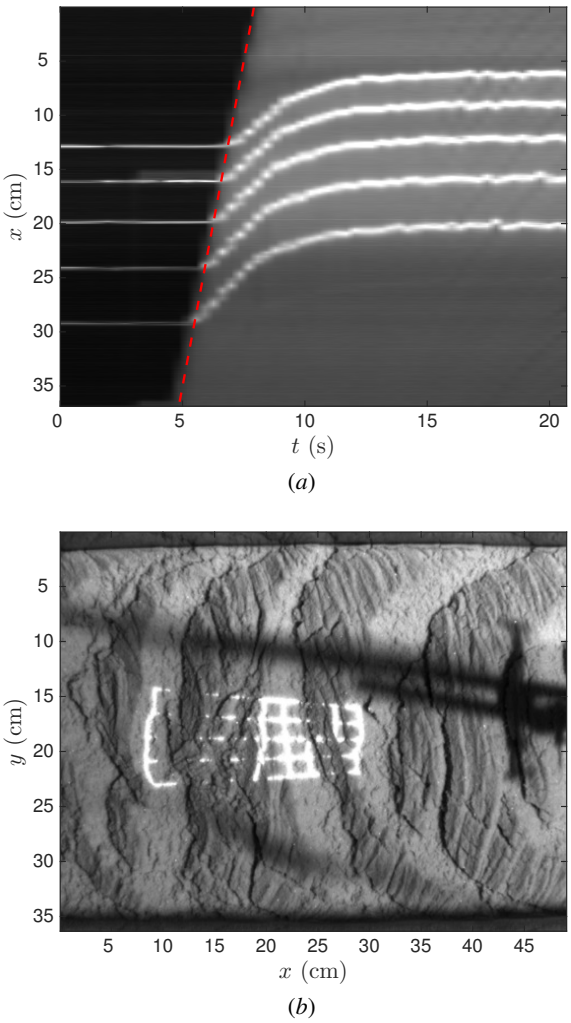

FIG. 2. (*a*) Time-space diagram showing the juxtaposition of a line of pixels for successive time steps t for $\theta = 29.5°$ and $f = 3.5$cm. This line of pixels is taken from a picture of the flow surface: it is longitudinal to the incline (along x) and crosses the flow front in its center. The red dashed straight line shows the front propagation at a constant velocity. (*b*) A picture of the free surface of a unsaturated wet granular layer deposited on the incline at $\theta = 30°$ and $f = 6$cm after the mass flow rate of a steady uniform flow was vanished.

rates and angles, the flow of (dry or unsaturated wet) grains is not continuous but intermittent, occurring by successive avalanches. For high enough mass flow rates and angles, a steady flow regime develops, characterized by the propagation of a (quasi-)constant thickness layer of (unsaturated wet or dry) grains throughout the rough plane. All our measurements will be done in the steady regime, far from the entrance and the exit of the plane and far from the front, where the flow is uniform: the free surface makes a constant angle longitudinally with the horizontal and is almost flat in the transverse direction.

The dense flows of unsaturated wet grains look like a continuous material, despite the presence of grain aggregates visible at surface in Fig. 1(b) and their probable existence inside the flow too. Just behind a slightly curved transverse interface showing small protuberances (not observed for a dry granular flow), the unsaturated wet granular layer exhibits some front profile, as shown by the white lines in Fig. 2(a). The granular layer propagates at a constant velocity denoted as u_0, as evidenced by the straight red dashed line, so this part of the flow is not uniform but steady. Behind this front, the thickness of the unsaturated wet granular layer, denoted as h, seems roughly uniform and steady. Also, a finer inspection shows small surface corrugations appearing systematically on the unsaturated wet granular layer [Fig. 1(b)], that are not observed for a dry granular flow.

Finally, upon the quick closing of the hopper gate, the flow velocity and thickness progressively decrease, leaving possibly a deposit on the incline. The unsaturated wet deposit morphology exhibits some characteristics that are not observed for the dry case, such as the coexistence of two different length scales related to the surface corrugations present during the flow and to fractures occurring during the arrest [Fig. 2(b)]. F

D. Measurement methods

In order to measure the mass flow rate Q_m, the mass m of grains flowing out of the inclined plane is weighted as a function of time thanks to a scale. The time evolution of the mass $m(t)$ of unsaturated wet grains ($\epsilon = 0.1\%$) is drawn in Fig. 3(a) for a given slope angle $\theta = 33°$ and different values of the gate height f. It is found that $m(t)$ is proportional to time and thus a constant mass flow rate Q_m can be defined. In the whole experimental range of f and θ explored here for different liquid contents ϵ, the mass flow rates varies from 1kg.s^{-1} to 10kg.s^{-1} for the dry sample ($\epsilon = 0$) and from 1kg.s^{-1} to 25kg.s^{-1} for the unsaturated wet grains. Figure 3(b) shows Q_m as a function of the hopper gate aperture f for different values of θ for a constant liquid content ($\epsilon = 0.5\%$): at given θ (or f), Q_m increases with f (or θ).

The central region of the rough inclined plane far from its entrance and its exit, in which the flow is almost uniform, is recorded by a CCD camera positioned at the normal of the plane at a 20Hz-frequency. The images and data are processed using ImageJ and Matlab. In this region, a grid pattern is projected on the plane by laser sheets [Fig. 1(b)], with a projection angle small enough so that the presence of any granular mass on the plane induces a significant deformation of the grid (Fig. 2). The local shift between the deformed grid pattern and the initial one without grains is proportional to the thickness $h(x, y, t)$ of the granular layer at the position x and y along the longitudinal and transverse direction and the time t[47]. The thickness h of the uniform steady flow is taken as the average of $h(x, y, t \to \infty)$ for all x and y in the central uniform region, so that the small variations of h maybe related to the presence of grain aggregates and corrugations at surface, are smoothed out.

The front velocity u_0 is obtained by tracking the front propagating down the incline thanks to a time-space diagram [Fig. 2(a)] which is the juxtaposition of a line of pixels for successive time steps, taken from a picture of the flow surface, along x (longitudinal to the incline) and crossing the

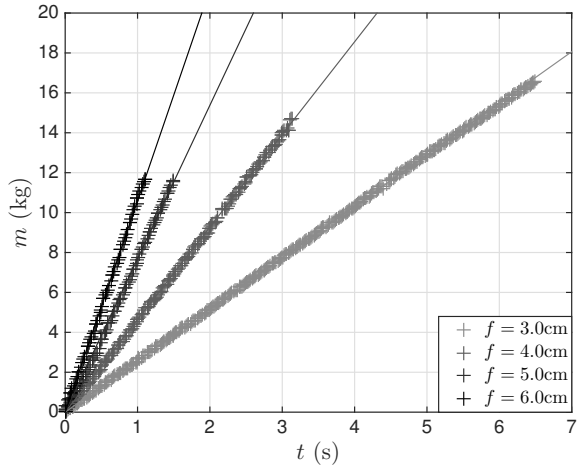

(*a*)

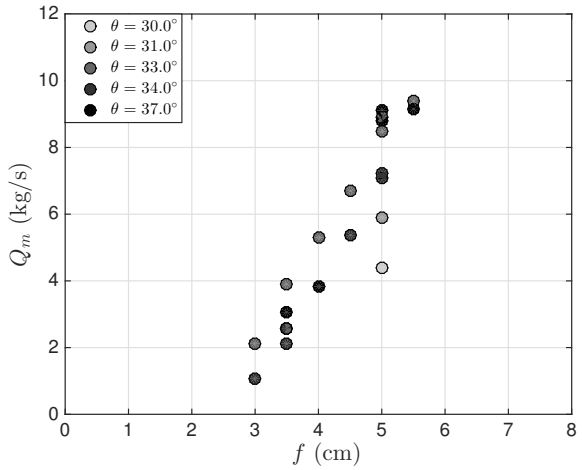

(*b*)

FIG. 3. (*a*) Temporal evolution of the mass $m(t)$ of unsaturated wet grains ($\epsilon = 0.1\%$) released out of the incline as a function of time for a series of experiments at a constant slope angle $\theta = 33°$ and for different aperture heights $f \in$ [3.0-6.0]cm. (*b*) The mass flow rate Q_m as a function of the hopper aperture height f for different incline slope angles $\theta \in$ [30.0-37.0]° for a constant liquid content $\epsilon = 0.5\%$.

flow front in its center ($y = W/2$). The mass balance equation $\partial h/\partial t + \partial(h\overline{u})/\partial x = 0$ with $\overline{u}$, the z-averaged velocity (z being the direction normal to the plane), applied to a front moving at a constant velocity u_0 without deformation, leads to a travelling wave $h(x,t) = h(x - u_0\,t)$, and implies $\overline{u} = u_0$[40]. Thus the front velocity u_0 and the velocity $\overline{u}$ averaged over z are equal.

The same measurements are done for unsaturated wet and dry granular flows.

We have checked that our measurements of h and u_0 are consistent with the independent measurement of the mass flow rate:

$$Q_m = \phi\,\rho\,W\,h\,u_0. \tag{7}$$

In the following, we will prefer to use measurements of Q_m instead of u_0 (in addition to h), because this former is less sensitive to experimental noise, thanks to its integration in time and space. We realized about 100 experiments of steady uniform dry granular flows and 30 experiments for the liquid content $\epsilon = 0.5\%$, while about 15 experiments for each other liquid content ϵ.

The scope of this paper is the study of the steady and uniform unsaturated wet granular flow regime down an incline. In addition to the liquid content ϵ, the control parameters are varied: the frontal gate opening height f between 0.5cm and 6cm and the incline slope angle θ between 24° and 39°, that will change the constant mass flow rate Q_m, the constant thickness h of the flow and the apparent friction μ^{app}.

III. EXPERIMENTAL RESULTS AND THEORETICAL PREDICTIONS

A. Flow threshold

Figure 4(a) shows the thickness h of steady uniform flows for the different slope angles θ explored for both the dry (squares) and the unsaturated wet (circles) granular samples for $\epsilon = 0.5\%$, the colors encoding for the values of the gate opening height f. Steady uniform flows are achieved for large enough values of h (or the gate opening height f) and θ. Increasing the gate opening height f leads to thicker flows down the incline and one can see that unsaturated wet granular flows are much thicker than dry ones. Indeed minima of h (and θ) for unsaturated wet granular flows are larger than the ones for dry granular flows.

As we did not observe any steady uniform dry granular flows for slopes smaller than $24.6 \pm 0.5°$, we identify the angle threshold $\theta_0 = 24°$ and get $\mu_0 = \tan(\theta_0) = 0.45$ for the static internal friction coefficient, represented by the dashed line in Fig. 4(a). The value of μ_0 aligns with measurements obtained from $h_{stop}(\theta)$[40,47,48] that are not shown here. h_{stop} represents the average thickness of deposits of dry grains following a steady, uniform flow at a slope angle θ, and the measurements were taken after a sudden closure of the silo. The value is also in agreement with rheological data of $\mu(I)$ (Fig. 10) and $Q_m(I)$ as made later in section III C. In the following, μ_0 is kept constant equal to 0.45 and will not be a free parameter anymore.

It is well established that steady and uniform flows are observed down a rough wide inclined plane for dry or immersed granular materials[24,26,47]: here, we obviously observe such steady uniform flows with dry grains, from which we will characterize their rheological parameters in section III C.

For unsaturated wet grains, we do also observe experimentally a steady state and uniform regime with a finite and (quasi-) constant thickness layer propagating along the rough inclined plane, which angle of the free surface is equal to the slope angle θ, for high enough mass flow rates Q_m and slope angles θ.

By referring the direction normal to the plane as z, the momentum equations for a steady free surface flow down an

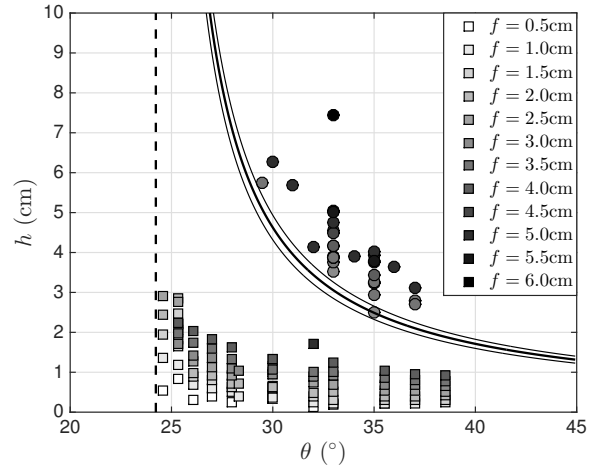

(*a*)

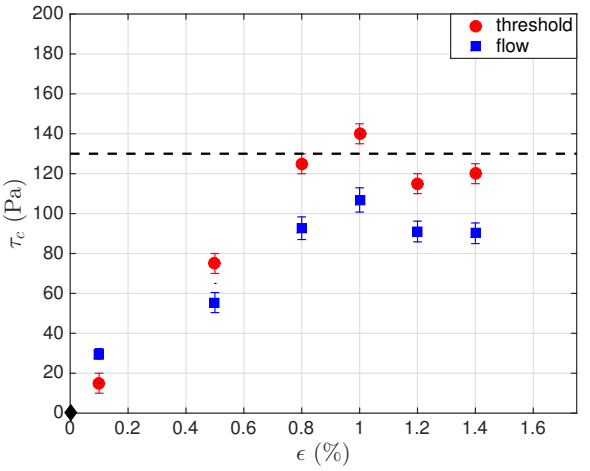

(*b*)

FIG. 4. (*a*) Parameters space (θ, h) of some experiments reported in this paper, with θ the incline slope angle and h the constant thickness of the unsaturated wet for $\epsilon = 0.5\%$ (circles) and dry (squares) granular flows. The colors encode for the values of the gate opening height f. The dashed line corresponds to the angle threshold $\theta_0 = \arctan(\mu_0)$. The continuous curve $h_c(\theta)$ (and the two enveloping curves) is computed from Eq. (11) with $\tau_c = 75 \pm 5$Pa and $\mu_0 = 0.45$, for the thickness threshold for a cohesive steady uniform free-surface gravitational flow. (*b*) Cohesion stress τ_c as a function of the mass liquid content ϵ, measured in two different ways: from the flow threshold data (h-θ) by using Eq. (11) (red circles) and from the (P, τ) data of steady uniform inertial flows (blue squares). The error bars are ±5Pa for the red circles, while they correspond to variations of ±0.01 around $\mu = 0.55$ for the blue squares. The dotted horizontal line indicates the cohesion stress according to the Rumpf model (12).

inclined plane at an angle θ give:

$$P(z) \simeq \phi(z)\rho g(h-z)\cos\theta, \tag{8}$$

$$\tau(z) \simeq \phi(z)\rho g(h-z)\sin\theta, \tag{9}$$

with τ and P, the shear and normal stresses at the position z. This leads to values for the reduced pressure P^* between 0.5 and 3 or for the cohesion index $1/P^*$ between 0.3 and 2, when computed in $z = 0$.

Thus, in case of a steady uniform flow, the inclined plane configuration, whatever the rheology is (viscous, granular, cohesive, ...), allows to control the apparent friction throughout the whole layer thickness:

$$\mu^{app} = \frac{\tau(z)}{P(z)} = \tan\theta. \tag{10}$$

In general, a yield stress τ_Y (so that the shear rate $\dot{\gamma} \neq 0$ for a shear stress $\tau \geq \tau_Y$) leads to the emergence of a length scale $h_Y = \tau_Y/\rho g \sin\theta$, as a thickness threshold for shear in a steady uniform gravitational flow of density ρ. In a similar way, cohesion in a granular material following Eq. (1) or (6), induces a yield stress $\tau_Y = \tau_c + \mu_0 P$, leading to a thickness threshold h_c for shear in a steady uniform gravitational flow of density $\phi(z=0)\rho \simeq \phi\rho$:

$$h_c = \frac{\tau_c}{\phi(z=0)\rho g\cos\theta}\frac{1}{\tan\theta - \mu_0}, \tag{11}$$

with μ_0, the static internal friction of the granular material, that was shown to be the same with or without liquid, either saturated or unsaturated[3,7,35]. This means that a steady uniform shear flow should occur only for cohesive granular layers thicker that the thickness threshold h_c; such a cohesive granular layer (of thickness $h \geq h_c$) will experience some shear at the bottom on the height $h - h_c$ and develop a plug velocity profile of height h_c above it. Note that h_c is proportional to the cohesion length ℓ_c[11,12], and $h_c(\theta = 90°) = \ell_c/\phi$.

The relation (11) for the thickness threshold $h_c(\theta)$ for cohesive granular flows ($epsilon = 0.5\%$) is drawn as the continuous line (and the two enveloping curves) for $\mu_0 = 0.45$ and $\tau_c = 75 \pm 5$Pa in Fig. 4(a). This later is identified so that the line $h_c(\theta)$ is just below the minimal values of (θ, h) for the steady uniform unsaturated wet granular flows reported here, and seems to describe well the yield threshold. We are highly confident in this identification because we reduced the gate opening height f to the minimum possible value for a given θ, until continuous flow was no longer observed. In the worst-case scenario, the values we obtained are only upper limits. The curve $h_c(\theta)$ separates the region of steady, uniform flow from the region where no steady, uniform flow can be achieved.

Due to the fact that the minimum flowing thickness $h_c(\theta)$ increases and diverges as the slope angle approaches the threshold θ_0, it becomes extremely difficult to maintain a steady, uniform flow of unsaturated wet granular materials at small angles $\theta \geq \theta_0$, as it would require much larger values for thickness h, gate height f, and mass flow rate Q_m, which are not feasible within our experimental set-up. Therefore, the minimum angle θ required to maintain unsaturated wet granular flows in our experiments appears to be larger than that required for dry granular flows.

The cohesion stresses τ_c measured for different mass liquid contents ϵ are plotted as red circles in Fig. 4(b) as a function of ϵ, with error bars taken equal to ±5Pa. A liquid content as small as $\epsilon = 0.1\%$ already induces cohesion properties, with a cohesion stress $\tau_c \simeq 30$Pa. Notice that in the pendular regime, the cohesion stress increases when increasing the liquid bridge

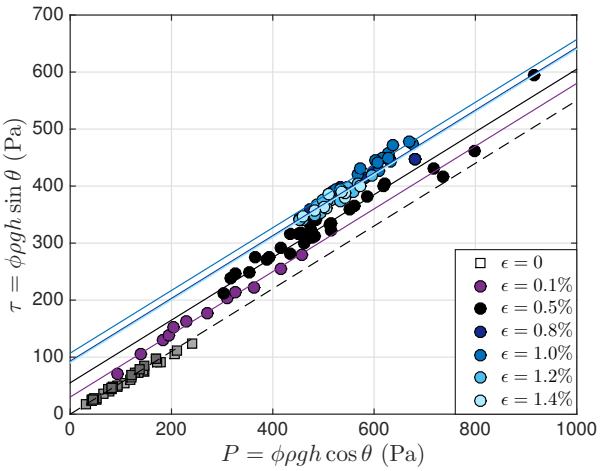

FIG. 5. Shear and normal stresses τ and P for the unsaturated wet flows at different $\epsilon \in [0.1\%\text{-}1.4\%]$ at all explored slopes θ (circles) and dry flows (squares) at slopes $\theta \in [27°\text{-}30°]$, so that they have approximately all the same internal friction $\mu \in [0.5\text{-}0.6]$.

volume[49,50]. Different amounts of liquid lead to different distributions of the liquid between the grains, and thus in turn lead to different values of the cohesion stress τ_c. We see that τ_c increases as the liquid content ϵ is increased and saturates for $\epsilon \simeq 0.8\%$ at a maximum of approximately 130Pa. This result is consistent with the cohesion stress of unsaturated wet glass beads measured in static shear strength experiments[1,42,51].

The maximal value of τ_c is often estimated by the Rumpf model[52]:

$$\tau_c = \frac{\mu_0 Z \phi \Gamma}{d}, \tag{12}$$

where Z is the "cohesive" coordination number, that is the average number per grain of contacts and distant pairs with capillary forces. If we estimate $Z \simeq 6$, $\phi \simeq 60\%$ and $\mu_0 = 0.45$, a cohesion stress $\tau_c \simeq 130$Pa is found, plotted as a dashed line in Fig. 4(b), that describes well the maximal and plateau value of τ_c we found. Note that the cohesion stress in the Rumpf model (12) is related to the Bond number Bo.

Besides this saturation, Raux and Biance [44] reported a second increase of τ_c with the liquid content, for even larger liquid contents than studied here.

In section III B, we will examine whether the cohesion stress τ_c, which characterizes the yield threshold for steady, uniform unsaturated wet granular flows down an inclined plane, is consistent with measurements of the cohesion stress observed during inertial flows.

B. Inertial flows: Cohesion stress

We now turn to the inertial granular flows by plotting in Fig. 5 the coordinates (P, τ) –the pressure [Eq. (8)] and the shear stress [Eq. (9)] at the bottom ($z = 0$)– for our materials at different liquid contents: some data at $\epsilon = 0$ and all data at $\epsilon \in [0.1\%\text{-}1.4\%]$. For a fixed non-zero value of ϵ, our data collected at various slope angles θ and gate opening heights f exhibit a nearly linear relationship, indicating that they possess a similar internal friction coefficient μ. It is worth noting that the changes in the internal friction coefficient $\mu(I)$ with respect to I are minimal, and as such, cannot be distinguished from a constant value in our analysis. Furthermore, the lines representing the linear relationship for different values of $\epsilon \neq 0$ are nearly parallel to each other, suggesting that these flows possess an internal friction coefficient that is approximately constant and equal to $\mu \simeq 0.55$. For comparison, (P, τ) is plotted for a selection of our dry samples (squares): those which friction is about $\mu \simeq 0.55$ (for slopes $\theta \in [27°\text{-}30°]$). As expected from Fig. 4(a), (P, τ) data of the dry glass beads lie below the unsaturated wet ones, because they are at smaller h and θ: this indicates that the apparent friction μ^{app} of the unsaturated wet beads is higher than the dry ones, even if their internal friction μ is approximately the same.

Also, when $\epsilon \neq 0$ (circles), our experimental data highlight a well defined non-zero cohesion stress $\tau_c(\epsilon)$ as the intersection of each line (for each ϵ) with the vertical $P = 0$-axis. The same plot for our dry samples (squares) shows obviously no cohesion stress ($\tau_c = 0$). We precise that, for a given ϵ, $\tau_c(\epsilon)$ is measured as the y-intercept of the affine fit of (P, τ) data when imposing the slope as $\mu = 0.55$ and its error bar (between 3 and 5Pa) is computed when imposing $\mu = 0.55 \pm 0.01$ [Fig. 4(b)].

We observe in Fig. 4(b) that the values of the measured cohesion stress τ_c (blue squares) from inertial flow experiments (Fig. 5) are approximately the same as that obtained for the flow threshold using Eq. (11) for the different liquid contents ϵ.

Thereby, we demonstrated that within the range of the experimental parameters explored here, each flow experiment being described by the maximal values of P and τ at the bottom plate ($z = 0$), a constant cohesion stress $\tau_c(\epsilon)$ at a given ϵ, is relevant from a rheological point of view, even for inertial flows, and not only for quasi-static plastic flows.

It appears that a cohesive Mohr-Coulomb criterion, such as Eq. (1) or (6), is applicable not only at the failure threshold[14], but even above it. This could be attributed to the slight variations of the internal friction coefficient μ with respect to the inertial number I in the case of our free-surface gravity-induced flows. Interestingly, this observation is consistent with the numerical simulations of cohesive plane shear by Berger *et al.* [6], where a dependence (albeit decreasing) of the cohesion stress $\tau_c(I)$ on the inertial number I is reported. However, in our study, the variation of the inertial number I is relatively low (one order of magnitude, as discussed later in section III E), such that the expected variation in the cohesion stress τ_c is even lower (a maximum of a factor of 1.5).

C. Inertial number dependence

We have shown that for the liquid contents ϵ explored here, our unsaturated wet granular flows down a rough incline are well described by the relation $\tau = \tau_c(\epsilon) + \mu P$, consistently with our dry granular flows described by $\tau = \mu P$, by carefully

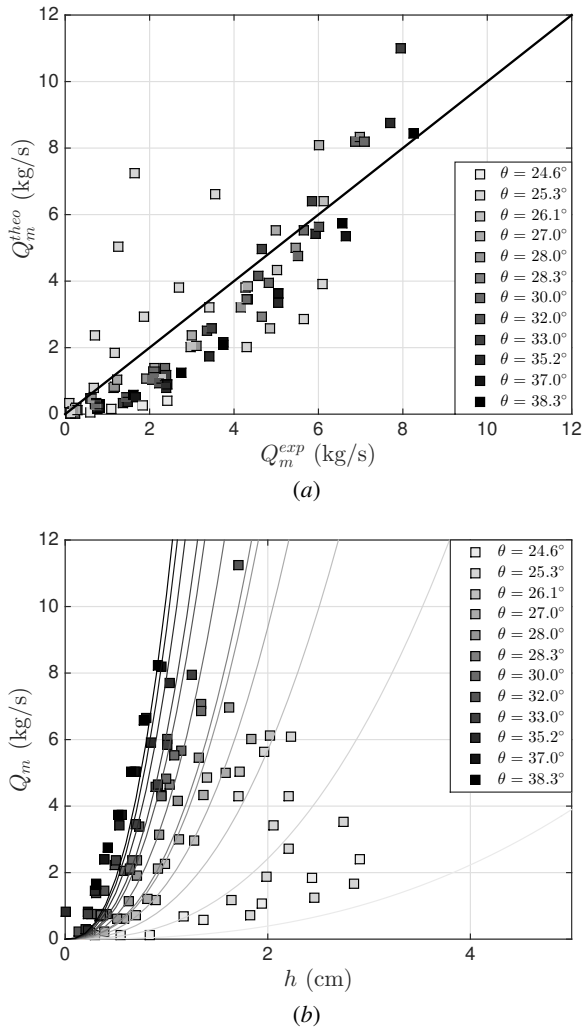

FIG. 6. Dry granular flows: (*a*) Theoretical values of the mass flow rate Q_m as a function of the experimental ones for the rheological parameters $\mu_0 = 0.46$ and $a = 0.7$ optimizing their linear correlation; (*b*) Mass flow rate Q_m experimentally measured as a function of the thickness of the steady uniform granular flow h and its prediction from Eq. (19).

considering dry and unsaturated wet flows at approximately the same internal friction μ. This allowed us to measure the cohesion stress $\tau_c(\epsilon)$ in the case of inertial flows, as the variations of the internal friction with the inertial number I were small. Now, we will consider possible variations of μ with I.

To be able to do further predictions on unsaturated wet granular flows, we assume that the rheology obeys Eq. (6) – with $\tau_c(I) = \tau_c(\epsilon)$ being constant at a given ϵ– and that the internal friction $\mu(I)$ follows an affine increasing function:

$$\mu(I) = \mu_0 + aI, \tag{13}$$

where μ_0 and a are two material-dependent parameters. We will show in Appendix A that the affine function and the more elaborate function with three parameters[31] lead approximately to the same results in the range of our experimental control parameters.

Thus in the case of a gravity-induced free surface steady uniform flow, Eqs. (10) and (13) allow to compute the local inertial number $I(z)$ in the sheared region for $z \leq h - h_c$, as:

$$I(z) = \frac{\tan\theta - \mu_0}{a} \frac{h - h_c - z}{h - z}, \tag{14}$$

while $I(z) = 0$ in the plug region for $z \geq h - h_c$. For a constant h (or θ), the function $I(z)$ is larger for a larger θ (or h). For a cohesionless material ($h_c = 0$), one retrieves a constant I in the sheared layer, whereas for a cohesive one, at a given (h, θ), the inertial number is maximal at the bottom:

$$I^{max} = I(z = 0) = \frac{\tan\theta - \mu_0}{a} \frac{h - h_c}{h}. \tag{15}$$

The relations (4), (11) and (14) give the following equation for the shear rate $\dot\gamma(z)$ for $z \leq h - h_c$:

$$\dot\gamma(z) = \frac{1}{d} \frac{\tan\theta - \mu_0}{a} \sqrt{\phi g \cos\theta} \left((h - z)^{1/2} - h_c \, (h - z)^{-1/2} \right), \tag{16}$$

while $\dot\gamma(z) = 0$ for $z \geq h - h_c$.

By integrating Eq. (16), assuming a no slip velocity at the bottom ($z = 0$) and a uniform profile of solid fraction $\phi(z) \simeq \phi$[13,14], we can compute the velocity field $u(z)$ for $z \leq h - h_c$ as:

$$\frac{u(z)}{\sqrt{gd}} = 2 \frac{\tan\theta - \mu_0}{a} \sqrt{\phi \cos\theta} \times \left(\frac{1}{3} \frac{h^{3/2} - (h - z)^{3/2}}{d^{3/2}} - \frac{h_c}{d} \frac{h^{1/2} - (h - z)^{1/2}}{d^{1/2}} \right), \tag{17}$$

while $u = u_c = u(z = h - h_c)$ for $z \geq h - h_c$. For a cohesionless material ($h_c = 0$), one retrieves the Bagnold velocity profile ($z^{3/2}$). For a cohesive material, the velocity profile can be viewed as the contribution of a Bagnold-type profile induced by its frictional properties and a second (negative) contribution ($z^{1/2}$) induced by its cohesion properties in the sheared layer ($z \leq h - h_c$), in addition to a plug profile (u_c) in the non-sheared top layer ($z \geq h - h_c$).

The mass flow rate [Eq. (7)] follows:

$$Q_m = \frac{2}{3} \frac{\tan\theta - \mu_0}{a} \frac{\phi \rho W \sqrt{g \phi \cos\theta}}{d} \times \left(\frac{3}{5} h^{5/2} - h_c h^{3/2} + \frac{2}{5} h_c^{5/2} \right), \tag{18}$$

that becomes, for cohesionless dry granular flows ($h_c = 0$):

$$Q_m(h_c = 0) = \frac{2}{5} \frac{\tan\theta - \mu_0}{a} \frac{\phi \rho W \sqrt{g \phi \cos\theta}}{d} h^{5/2}. \tag{19}$$

The characteristic inertial number I of the flow, chosen as its maximal value I^{max} [Eq. (15)], is related to the experimental measurements Q_m and h as:

$$I \equiv I^{max} = \frac{3}{2} \frac{1}{\sqrt{\phi \cos\theta}} \frac{Q_m}{Q_{m\,0}} \frac{h - h_c}{h} \times \frac{d^{5/2}}{3h^{5/2}/5 - h_c h^{3/2} + 2h_c^{5/2}/5}, \tag{20}$$

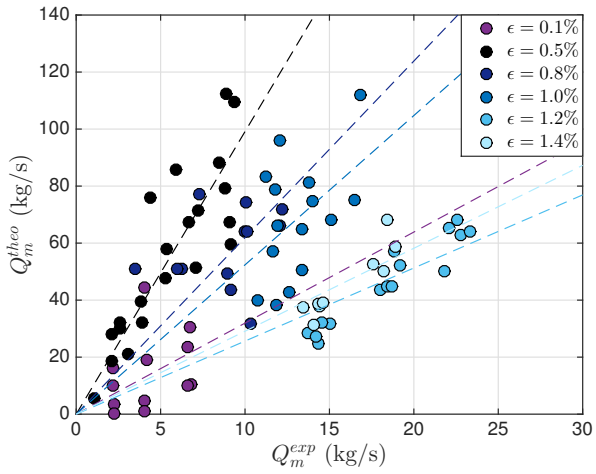

(*a*)

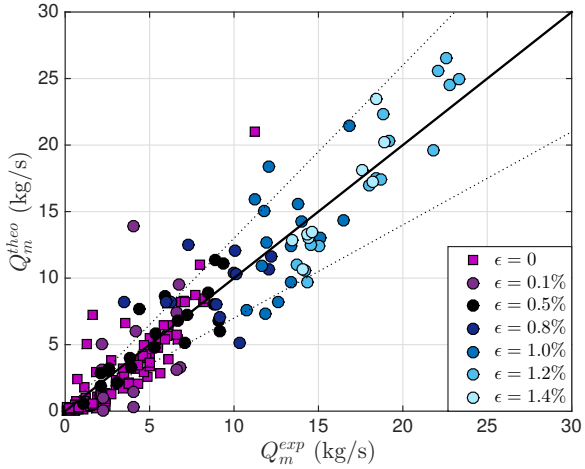

(*b*)

FIG. 7. Theoretical and experimental values of the mass flow rate Q_m for our unsaturated wet flows using Eq. (18) using the grain size d in (*a*) and Eq. (23) using the grain aggregate size d_{agg} in (*b*). In (*a*), the dashed lines corresponding to linear fits are guides for the eye. In (*b*), the continuous line has the slope 1, while the dotted lines have slopes 0.7 and 1.3, allowing us to compute the upper and lower error bars made on each measurement of d_{agg} (see the text).

with $Q_{m0} = \phi\rho W d\sqrt{gd}$, that becomes, for cohesionless dry granular flows ($h_c = 0$):

$$I_{dry} \equiv I^{max}(h_c = 0) = \frac{5}{2}\frac{1}{\sqrt{\phi\cos\theta}}\frac{Q_m}{Q_{m0}}\frac{d^{5/2}}{h^{5/2}}. \qquad (21)$$

Equation (20) indicates that the velocity profile (17) specific to cohesive flows hinders the direct computation of the characteristic inertial number I from experimental measurements without prior knowledge of certain rheological parameters (τ_c and μ_0 required for h_c), making it necessary to resort to alternative methods for the identification of the rheological law. It is worth noting that the knowledge of a is not essential in this regard.

The next step is to quantitatively identify the parameters of the friction law $\mu(I)$ in Eq. (13) from the dry granular flows made of the same glass beads as in our unsaturated wet materials. We identify our parameters (μ_0, a) as the ones optimizing the correlation between the theoretical –from Eq. (19)– and experimental values of the mass flow rate Q_m of our dry granular flows. This optimization is possible thanks to a decoupling of μ_0 and a: the linear relation between theoretical and experimental Q_m [Fig. 6(a)] has its slope related to a only, while its scattering (quantified by the precision of a linear fit) is related to the value of μ_0 only.

This leads for our dry granular flows to $\mu_0 = 0.46$ and $a = 0.7$, consistent with values found for glass beads of the same order of size[40]. Moreover, the static friction μ_0 is approximately the same as that obtained for the flow threshold in section III A [Fig. 4(a)]. We will see in Fig. 10 that this affine function describes very well our dry data $\mu(I)$ and the direct fit gives the same values for (μ_0, a).

For these rheological parameters, the theoretical values of the mass flow rate are plotted as a function of the experimental ones for our dry granular flows in Fig. 6(a). Figure 6(b) shows the predicted curves of the mass flow rate Q_m for our dry granular flows as a function of the granular layer thickness h (continuous lines) from Eq. (19) for different slope angles θ: the quantitative agreement with our experimental measurements (squares) is quite good.

Moreover, we have checked that the expected variation of the solid fraction ϕ with the inertial number I (according to $\phi(I) = \phi_{RCP} - \Delta\phi\, I$ with typical values of $\Delta\phi = 10\%$ and $\phi_{RCP} \simeq 60\%$ from the literature) implemented to compute the theoretical mass flow rate, does not change our results.

D. Aggregate size

Now let's consider the case of unsaturated wet. In this case, the shear flow is localized and not reduced to a Bagnold profile, leading to Eq. (18) for the mass flow rate Q_m. When we compute it with the previously identified parameters for $\mu(I)$ and τ_c, one can see, in Fig. 7(a), for each liquid content ϵ, a quite linear correlation between theoretical and experimental data. However, theoretical data over-estimate our measurements: each slope for each value of ϵ is $\gg 1$ (between 2 and 10) and depends on the liquid content ϵ. At this point, there are several possible approaches to explain this misestimation of the mass flow rate Q_m in unsaturated wet flows. However, all these approaches agree with the presence of wet grain aggregates. So, we will focus on one interpretation that considers the aggregate size as the elementary length scale instead of the individual grain size d. This interpretation is supported by the fact that the aggregates would affect the relaxation time scale in the definition of the inertial number (4), which is usually based on the assumption of cohesionless grains[24].

Indeed, while shearing a dense cohesionless granular material requires the displacement and relaxation of each single grain relative to its close neighbours, shearing a cohesive granular material will require the displacement and relaxation of grain aggregates[13]. Subsequently, the relaxation mechanisms must be considered at the scale of grain aggregates of size

d_{agg}, rather than at the scale of single grains. Hence, the effect of cohesion and grain aggregates would be to increase the elementary free-fall relaxation time (to be compared to the typical time of deformation), and accordingly to increase the inertial number and modify it into I_{agg}:

$$I_{agg} = \frac{\dot{\gamma} d_{agg}}{\sqrt{P/\rho}}. \tag{22}$$

Thus, when taking into account aggregates in the analysis made in Section III C, the mass flow rate would be given by:

$$Q_m = \frac{2}{3}\frac{\tan\theta - \mu_0}{a}\frac{\phi\rho W\sqrt{g\phi\cos\theta}}{d_{agg}} \times\left(\frac{3}{5}h^{5/2} - h_c h^{3/2} + \frac{2}{5}h_c^{5/2}\right), \tag{23}$$

leading to the relation of I_{agg} as a function of our experimental measurements Q_m and h:

$$I_{agg} = \frac{3}{2}\frac{1}{\sqrt{\phi\cos\theta}}\frac{Q_m}{Q_{m\,0\,agg}}\frac{h-h_c}{h} \times\frac{d_{agg}^{5/2}}{3h^{5/2}/5 - h_c h^{3/2} + 2h_c^{5/2}/5} \tag{24}$$

with $Q_{m\,0\,agg} = \phi\rho W d_{agg}\sqrt{g d_{agg}}$. Note that d_{agg} does not come into play in Eq. (24).

So, we identify the value of d_{agg} so as to get the collapse of theoretical *versus* experimental mass flow rates values Q_m, using Eq. (23): d_{agg} and its lower and upper bounds are such that the slope is 1 ± 0.3 (this uncertainty is chosen consistently with the scattering of our experimental measurements of Q_m). Figure 7(b) displays this "by-construction" collapse: the theoretical values of Q_m [Eq. (23)] dependent on d_{agg} is plotted as a function of our experimental values for the different liquid contents ϵ. Thus, the rheology (6) provides a good estimation of the mass flow rate for the unsaturated wet and for the dry materials, only when one introduces an aggregate size. Also Fig. 8 shows the predicted curves of the mass flow rate Q_m from Eq. (23) as a function of the granular layer thickness h (continuous lines) superimposed on our experimental data for different slope angles θ for two different liquid contents $\epsilon = 0.5\%$ and 1.2%.

The relative grain aggregate size d_{agg}/d plotted as a function of ϵ in Fig. 9, is not constant but is a function of the liquid content ϵ, as already observed for some characteristics of the microstructure of the wet granular materials[1,17,43]. Indeed, d_{agg}/d is not a monotonic function of ϵ, but displays a maximum at a critical value of $\epsilon \simeq 0.5\%$. This is surprising in light of the monotonic evolution of the cohesion stress τ_c and the induced cohesion length ℓ_c [Eq. (2)]. We will see that the mechanisms responsible for these two properties (aggregate size and cohesion) may have different origins.

It is known from X-ray microtomography[1] that the number of capillary bridges per particle depends of the liquid content: it increases rapidly at low ϵ before saturating at intermediate liquid contents; then, when the liquid content increases further, the number of capillary bridges vanishes to the detriment of

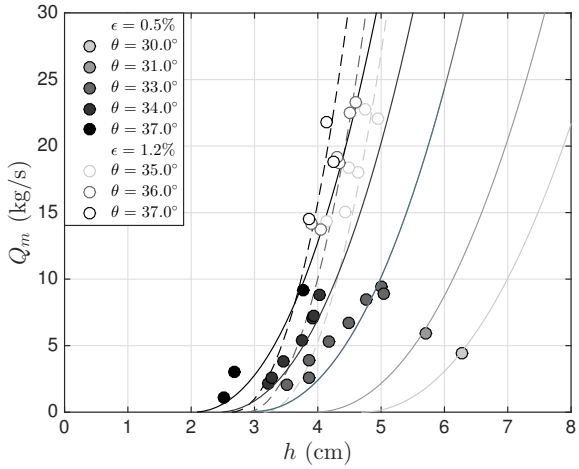

FIG. 8. Unsaturated wet granular flows: Mass flow rate Q_m experimentally measured as a function of the thickness of the steady uniform granular flow h and its predictions from Eq. (23) for $\epsilon = 0.5\%$ and 1.2%.

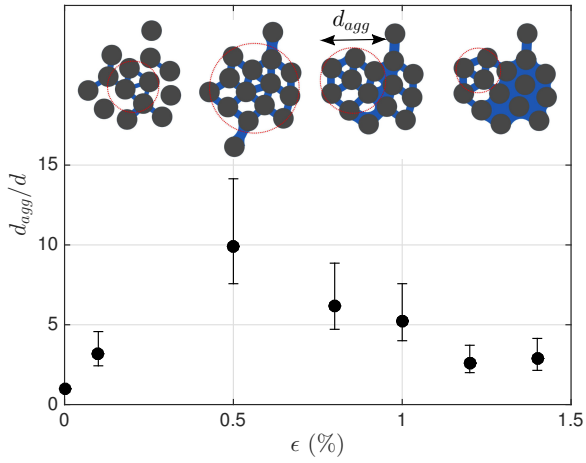

FIG. 9. The relative grain aggregate size d_{agg}/d as a function of the liquid content ϵ: d_{agg} and its lower and upper bounds are computed so that the linear fit slope of theoretical *versus* experimental values of the mass flow rate Q_m is 1 ± 0.3 (Fig. **??**). The inset shows sketches of a typical unsaturated wet grain aggregate for different liquid contents.

dimers, trimers and larger liquid/grain clusters, because the liquid invades and saturates some pores[1,2]. In the same time, the cohesion stress increases rapidly before saturating at a maximum, which we observed as shown in Fig.4(b).

Following the approach of Courrech du Pont *et al.* [53] in the case of Van der Waals attractive forces, we can estimate the size d_{agg} of the aggregates by considering an additional bead to belong to the aggregate only if its cohesive force is greater than its own weight added to the weight of the aggregate. Assuming that the cohesive force is proportional to the number of capillary liquid bridges n (through a coefficient $\alpha \leq 1$), given by $F_c = \alpha n \pi \Gamma d$, and the weight to balance is $W = \phi\rho\pi g (d_{agg})^3/6$, we obtain the following expression for the

aggregate size d_{agg}:

$$d_{agg} = \left(\frac{6\alpha n \Gamma d}{\phi \rho g}\right)^{1/3}, \tag{25}$$

if $\Gamma \neq 0$ and $n \neq 0$, and $d_{agg} = d$ otherwise.

The coefficient α determines the proportion of liquid bridges that are involved in binding a grain to an aggregate. As it is likely that only a fraction of the liquid bridges contributes to the cohesive force, α is expected to be less than or equal to 1. It is expected that $\alpha = 1/2$, indicating that only half of the liquid bridges are involved in binding a grain to an aggregate. However, as α appears with an exponent of $1/3$ in Eq. (25), small variations in the value of α do not significantly affect the predicted aggregate size d_{agg}. Then, by using the experimental data of the number of simple capillary bridges (binding two particles) from Scheel *et al.*[1]: $n \in [1,6]$, we get $d_{agg}/d \in [4,9]$, that is in quantitative agreement with our measurements in Fig. 9. However, despite this, determining the function $d_{agg}/d(\epsilon)$ is challenging as it requires the knowledge of the relevant parameter on which n depends. Additionally, our study highlights that the heterogeneous spatial distribution of liquid among grains plays a crucial role in the formation of grain aggregates, which size defines an additional length-scale in the system. The number of liquid bridges and their properties could potentially be used to define the size of these aggregates.

The such defined unsaturated wet grain aggregates is made of grains bonded by the strongest capillary forces (*i.e.* simple capillary bridges), with its interface separating them from liquid/grain/air clusters, and the size d_{agg} is defined as the mean size of such aggregates. Whereas the aggregates are related to the contribution of the n strongest bounds, the cohesion is induced by the contribution of all of the Z cohesive bounds (contacts and distant pairs with capillary forces): $Z \simeq n + n_2 + n_3 + ... n_{max}$ is the sum of the number of simple liquid bridges and liquid/grain/air clusters, involving two, three, four, ... particles, *i.e.* the capillary bridges, dimers, trimers and larger liquid/grain clusters[1,2,54–57]. Furthermore, one can see from the experimental measurements[1,43] that n increases, then decreases, while $n + n_{max} \approx Z$ increases, then saturates with the liquid content. This explains why only the n simple capillary bridges come into play in Eq. (25), while all the Z cohesive bounds come into play in Eq. (12). Interestingly, the different mechanisms responsible for the cohesion and for the aggregates in case of capillary-induced cohesion, explain that the size of our aggregates does not scale with the cohesion length ℓ_c[11,12]. This raises the open question of the size of aggregates in other cohesive granular flows, in case of cohesion of another nature than capillary[2,11,14,36,58]. Note that our measurements of d_{agg} are indirect, so they appeal for future studies.

E. Internal friction

We have now identified the rheology (6) and its parameters (τ_c, μ_0, a), successfully describing our experimental measurements, when coupled with the grain aggregate size (25). We will plot the internal friction coefficient μ as a function of the inertial numbers I and I_{agg} defined either at the grain size d or at the aggregate size d_{agg} in Fig. 10(a) and (b) for our dry and unsaturated wet granular flows. The internal friction μ is equal to the apparent friction $\mu^{app} = \tan(\theta)$ for our dry flows, while for our cohesive flows, it is given by $\mu = \mu^{app} - \tau_c/P$. For dry flows, the inertial numbers I_{dry} and I_{agg} are equal (since $d_{agg} = d$ when $n = 0$ or $\Gamma = 0$) and is computed from Eq. (21). For cohesive flows, I and I_{agg} are computed respectively from Eqs. (20) and (24). We recall that Eq. (20) still holds, as long as the values identified for μ_0 and τ_c hold. One can note that, whatever the definition (I or I_{agg}), the inertial number typically changes between 10^{-2} and 1, corresponding to the dense inertial flow regime, above the quasi-static regime, for which the internal friction would tend to its quasi-static value μ_0.

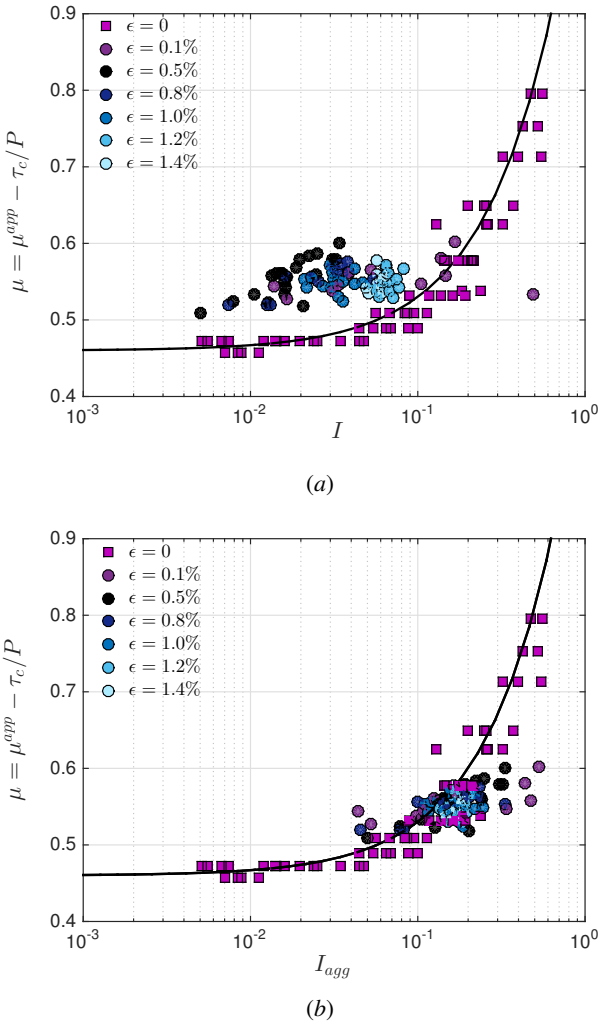

FIG. 10. Internal friction coefficient μ as a function of the inertial number I at the grain size d from Eq. (20) in (a) and I_{agg} defined at the aggregate size d_{agg} from Eq. (24) in (b) for unsaturated wet flows and Eq. (21) for dry ones.

The affine function (13) with the previously identified parameters (μ_0, a) plotted as a continuous line, provides an ex-

cellent description of our experimental measurements $\mu(I)$ (squares) for our dry flows. In Fig. 10(a), when the inertial number I is defined at the grain scale d, our measurements $\mu(I)$ for our unsaturated wet flows do not collapse with the dry data, nor for the different liquid contents $\epsilon \neq 0$.

In section III D, we analyzed the aggregates and found that, by construction, all of our experimental measurements approximately collapse when $\mu(I_{agg})$ is plotted. This is in contrast to $\mu(I)$, and it shows that the observed variations in the internal friction in the rheology (6) can be explained by the presence of aggregates.

However, although the cohesive data collapse well thanks to the introduction of I_{agg}, there are still slight deviations in the superposition of all cohesive data with dry data. This suggests that second-order mechanisms should be taken into account to further improve the collapse. One possible explanation for this is a slight modification of the internal friction due to the presence of liquid. To account for this modification, the physical properties of the liquid should be incorporated into the model, what still could be described using our approach, by considering the possible dependence of d_{agg} with the physical properties of the liquid and with the shear rate.

IV. CONCLUSION

To better understand cohesive granular materials, it is necessary to validate different rheological laws proposed in the literature[6,9,11,13,14,34–36] by comparing them with various datasets. Therefore, the development of experimental setups and data acquisition methods is an ongoing requirement. In this paper, we presented experiments involving the flow down a rough inclined plane of unsaturated wet cohesive granular materials, which are strongly affected by inter-grain cohesive forces. Our experimental data were successfully described by the following cohesive Mohr-Coulomb yield criterion extended to inertial flows:

$$\tau = \tau_c(\epsilon, Bo) + \mu(I_{agg}(\epsilon))\, P, \tag{26}$$

.

Here, τ_c is a cohesion stress dependent on the liquid content ϵ and the Bond number Bo, and $\mu(I_{agg})$ is an internal friction coefficient common to dry and unsaturated wet flows. The presence of wet grain aggregates is taken into account through their size $d_{agg}(\epsilon)$, which depends on ϵ, consistent with the growth of the microstructure observed in unsaturated wet granular materials[1,43]. This scenario needs future measurements of the different characteristic length scales of the flow and deposit morphologies, such as those observed in Fig. 2(b), which should be compared to d_{agg} and ℓ_c, the cohesion length (2).

The consideration of aggregates allows to retrieve the increase of the relaxation time that comes into play in the inertial number when cohesive bonds are present. One very promising rheology is the one proposed by Vo *et al.* [36]. However, this rheology predicts a smaller relaxation time with cohesion forces than without them and a larger relaxation time for a larger liquid viscosity, indicating that viscous effects rather than cohesive effects should allow us to retrieve our experimental data. All this underscores the need for systematic comparison of the rheology proposed in[36] with our and other available (experimental and numerical) measurements. Indeed, the liquid bonds also give rise to viscous forces when the grains flow: investigating the rheological effects of the variations in the viscosity and surface tension of the wetting liquid would help to identify the relevant rheological laws that account for capillary and viscous forces in addition to inertial effects.

Appendix A: The more elaborate function for $\mu(I)$

All the previous computations performed for the affine function $\mu(I)$ can be done for a more elaborate function:

$$\mu(I) = \mu_0 + \frac{\Delta\mu}{1 + \frac{I_0}{I}}, \tag{A1}$$

with three parameters as commonly used in the literature[31]. Such a function allows to describe the saturation of the internal friction with large inertial numbers, leading to some accelerating flows, contrary to the affine function. In this case, the inertial number follows as:

$$I^{3\,param.}(z) = I_0 \frac{h - h_c - z}{(h - z)(1/\delta - 1) + h_c} \tag{A2}$$

where $\delta = (\tan\theta - \mu_0)/\Delta\mu$, leading to the local shear rate:

$$\dot{\gamma}(z) = \frac{I_0}{d}\sqrt{\phi g \cos\theta}\frac{(h - z)^{1/2}(h - h_c - z)}{(h - z)(1/\delta - 1) + h_c} \tag{A3}$$

and the velocity field:

$$u(z) = k_1(h-z)^{3/2} + k_2(h-z)^{1/2} + k_3\ \arctan(k_4(h-z)^{1/2}) + k_5, \tag{A4}$$

with five constants k_i (with $i = 1, 2, 3, 4$ and 5) dependent on the parameters of the rheology and of the flow. However, the expressions are not so compact and easy to manipulate as previously, e.g. a term $k_3 \arctan(k_4(h - z)^{1/2})$ appears in the expression of $u(z)$. Most importantly, when we compare quantitatively theoretical predictions from these two different laws, there are only few non-significant differences in the range of our experimental values (Fig. 11).

If we define a in the affine function as $a = \Delta\mu/I_0$, with $\Delta\mu$ and I_0 from the more elaborate model, as suggested by an asymptotic development, then one systematically gets:

$$I^{3\,param.} = I^{aff.}\left(\frac{h - z}{h - z - \delta(h - h_c - z)}\right) \geq I^{aff.}, \tag{A5}$$

with

$$\delta = \frac{\tan\theta - \mu_0}{\Delta\mu}, \tag{A6}$$

that would lead to predictions from the elaborate model for velocities and mass flow rates, slightly larger than from the affine model.

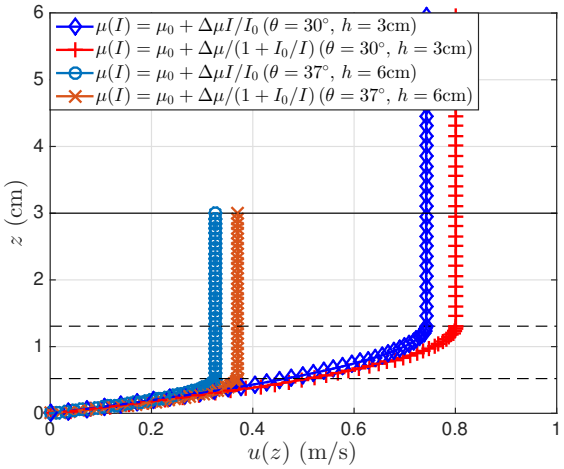

FIG. 11. Two examples of normal profiles $I(z)$ and $u(z)$ assuming either an affine function ($a = \Delta\mu/I_0$) or a more elaborate model for $\mu(I)$ with the parameters $I_0 = 0.38$, $\mu_0 = 0.41$ and $\Delta\mu = 0.35$ from[40] and $\tau_c = 100$Pa for ($\theta = 30°$, $h = 6$cm) and ($\theta = 37°$, $h = 3$cm).

ACKNOWLEDGMENTS

We want to thank Philippe Gondret for his interesting suggestion. We thank Thierry Bastien, Jean-Marie Citerne, Christophe Courrier, David Hautemayou and Cédric Mézière for technical helps with the experimental set-up. We also would like to acknowledge the students Emma Charanton, Samy Idrissi-Kaitouni, Périg Le Jeannic, Mathurin Romand, Hugo Sampieri and Khady Seck. We thank Anaïs Abramian, Pierre-Yves Lagrée, Jean-Noël Roux and Lydie Staron for insightful discussions. A. Fall thanks the Agence Nationale de la Recherche (Grant No. ANR-16-CE08-0005-01) for funding. S. Deboeuf thanks Camille Noûs from Laboratoire Cogitamus.

[1] M. Scheel, R. Seemann, M. Brinkmann, M. Di Michiel, A. Sheppard, and S. Herminghaus, "Liquid distribution and cohesion in wet granular assemblies beyond the capillary bridge regime," J. Phys. Condens. Mater. **20**, 494236 (2008).
[2] M. Badetti, A. Fall, D. Hautemayou, F. Chevoir, P. Aimedieu, S. Rodts, and J.-N. Roux, "Rheology and microstructure of unsaturated granular materials: Experiments and simulations," J. Rheol. **62**, 1175–1186 (2018).
[3] P. Pierrat, D. K. Agrawal, and H. S. Caram, "Effect of moisture on the yield locus of granular materials: theory of shift," Powder Technol. **99**, 220–227 (1998).
[4] J. A. S. Cleaver, R. M. Nedderman, and R. B. Thorpe, "Accounting for granular material dilation during the operation of an annular shear cell," Adv. Powder Technol. **11**, 385–400 (2000).
[5] J. K. Mitchell, K. Soga, *et al.*, *Fundamentals of soil behavior*, Vol. 3 (John Wiley & Sons New York, 2005).
[6] N. Berger, E. Azéma, J.-F. Douce, and F. Radjai, "Scaling behaviour of cohesive granular flows," EPL (Europhys. Lett.) **112**, 64004 (2015).
[7] F. Boyer, E. Guazzelli, and O. Pouliquen, "Unifying suspension and granular rheology," Phys. Rev. Lett. **107**, 188301 (2011).
[8] F. Tapia, O. Pouliquen, and É. Guazzelli, "Influence of surface roughness on the rheology of immersed and dry frictional spheres," Phys. Rev. Fluids **4**, 104302 (2019).
[9] P. G. Rognon, J.-N. Roux, D. Wolf, M. Naaïm, and F. Chevoir, "Rheophysics of cohesive granular materials," EPL (Europhys. Lett.) **74**, 644 (2006).
[10] L. Kovalcinova, S. Karmakar, M. Schaber, A.-L. Schuhmacher, M. Scheel, M. DiMichiel, M. Brinkmann, R. Seemann, and K. L., "Energy dissipation in sheared wet granular assemblies," Phys. Rev. E **98**, 032905 (2018).
[11] A. Abramian, L. Staron, and P.-Y. Lagrée, "The slumping of a cohesive granular column: Continuum and discrete modeling," J. Rheol. **64**, 1227–1235 (2020).
[12] A. Abramian, P.-Y. Lagrée, and L. Staron, "How cohesion controls the roughness of a granular deposit," Soft Matter **17**, 10723–10729 (2021).
[13] P. G. Rognon, J.-N. Roux, M. Naaim, and F. Chevoir, "Dense flows of cohesive granular materials," J. Fluid Mech. **596**, 21–47 (2008).
[14] S. Mandal, M. Nicolas, and O. Pouliquen, "Insights into the rheology of cohesive granular media," Proc. Nat. Acad. Sci. USA **117**, 8366–8373 (2020).
[15] N. Mitarai and F. Nori, "Wet granular materials," Adv. Phys. **55**, 1–45 (2006).
[16] S. Strauch and S. Herminghaus, "Wet granular matter: a truly complex fluid," Soft Matter **8**, 8271–8280 (2012).
[17] B. Andreotti, Y. Forterre, and O. Pouliquen, *Granular media: between fluid and solid* (Cambridge University Press, 2013).
[18] L. Bocquet, E. Charlaix, S. Ciliberto, and J. Crassous, "Moisture-induced ageing in granular media and the kinetics of capillary condensation," Nature (London) **396**, 735–737 (1998).
[19] M. Pakpour, M. Habibi, P. Møller, and D. Bonn, "How to construct the perfect sandcastle," Sci. Rep. **2**, 1–3 (2012).
[20] P. Tegzes, T. Vicsek, and P. Schiffer, "Development of correlations in the dynamics of wet granular avalanches," Phys. Rev. E **67**, 051303 (2003).
[21] R. Brewster, G. S. Grest, and A. J. Levine, "Effects of cohesion on the surface angle and velocity profiles of granular material in a rotating drum," Phys. Rev. E **79**, 011305 (2009).
[22] A. Jarray, V. Magnanimo, and S. Luding, "Wet granular flow control through liquid induced cohesion," Powder Technol. **341**, 126–139 (2019), continuous Manufacturing/Processing.
[23] N. Preud'Homme, G. Lumay, N. Vandewalle, and E. Opsomer, "Numerical measurement of flow fluctuations to quantify cohesion in granular materials," Phys. Rev. E **104**, 064901 (2021).
[24] GDRMiDi, "On dense granular flows," Eur. Phys. J. E **14**, 341–365 (2004).
[25] F. Da Cruz, S. Emam, M. Prochnow, J.-N. Roux, and F. Chevoir, "Rheophysics of dense granular materials: Discrete simulation of plane shear flows," Phys. Rev. E **72**, 021309 (2005).
[26] C. Cassar, M. Nicolas, and O. Pouliquen, "Submarine granular flows down inclined planes," Phys. Fluids **17**, 103301 (2005).
[27] G. Ovarlez, F. Bertrand, and S. Rodts, "Local determination of the constitutive law of a dense suspension of noncolloidal particles through magnetic resonance imaging," Journal of rheology **50**, 259–292 (2006).
[28] M. Trulsson, B. Andreotti, and P. Claudin, "Transition from the viscous to inertial regime in dense suspensions," Phys. Rev. Lett. **109**, 118305 (2012).
[29] L. Amarsid, J.-Y. Delenne, P. Mutabaruka, Y. Monerie, F. Perales, and F. Radjai, "Viscoinertial regime of immersed granular flows," Phys. Rev. E **96**, 012901 (2017).
[30] C. A. Coulomb, "Sur une application des règles de maximis et minimis à quelques problèmes de statique, relatifs à l'architecture," Mém. Math. Phys. **7**, 343–382 (1773).
[31] P. Jop, Y. Forterre, and O. Pouliquen, "A constitutive law for dense granular flows," Nature (London) **441**, 727–730 (2006).
[32] Y. Forterre and O. Pouliquen, "Flows of dense granular media," Annual Review of Fluid Mechanics **40**, 1–24 (2008).
[33] F. Gilabert, J.-N. Roux, and A. Castellanos, "Computer simulation of model cohesive powders: Influence of assembling procedure and contact laws on low consolidation states," Physical review E **75**, 011303 (2007).
[34] S. Khamseh, J.-N. Roux, and F. Chevoir, "Flow of wet granular materials: A numerical study," Phys. Rev. E **92**, 022201 (2015).
[35] M. Badetti, A. Fall, F. Chevoir, and J.-N. Roux, "Shear strength of wet granular materials: macroscopic cohesion and effective stress – discrete numerical simulations, confronted to experimental measurements," Eur. Phys. J. E **41**, 68 (2018).
[36] T. T. Vo, S. Nezamabadi, P. Mutabaruka, J.-Y. Delenne, and F. Radjai, "Additive rheology of complex granular flows," Nature Comm. **11**, 1–8 (2020).
[37] S. B. Savage, "Granular flows down rough inclines - review and extension," in *Mechanics of Granular Materials*, Studies Applied Mech., Vol. 7, edited by J. T. Jenkins and M. Satake (Elsevier, 1983) pp. 261 – 282.

[38] S. B. Savage, "The mechanics of rapid granular flows," in *Adv. Applied Mech.*, Vol. 24 (Elsevier, 1984) pp. 289–366.
[39] O. Pouliquen and N. Renaut, "Onset of granular flows on an inclined rough surface: dilatancy effects," J. Phys. II **6**, 923–935 (1996).
[40] G. Saingier, S. Deboeuf, and P.-Y. Lagrée, "On the front shape of an inertial granular flow down a rough incline," Phys. Fluids **28**, 053302 (2016).
[41] R. Brewster, G. S. Grest, J. W. Landry, and A. J. Levine, "Plug flow and the breakdown of bagnold scaling in cohesive granular flows," Phys. Rev. E **72**, 061301 (2005).
[42] Z. Fournier, D. Geromichalos, S. Herminghaus, M. M. Kohonen, F. Mugele, M. Scheel, M. Schulz, B. Schulz, C. Schier, R. Seemann, *et al.*, "Mechanical properties of wet granular materials," J. Phys.: Condens. Matter **17**, S477 (2005).
[43] M. Scheel, R. Seemann, M. Brinkmann, M. Di Michiel, A. Sheppard, B. Breidenbach, and S. Herminghaus, "Morphological clues to wet granular pile stability," Nat. Mater. **7**, 189–193 (2008).
[44] P. S. Raux and A.-L. Biance, "Cohesion and agglomeration of wet powders," Phys. Rev. Fluids **3**, 014301 (2018).
[45] P. Jop, Y. Forterre, and O. Pouliquen, "Crucial role of sidewalls in granular surface flows: consequences for the rheology," J. Fluid Mech. **541**, 167–192 (2005).
[46] E. Freyssingeas, M.-J. Dalbe, and J.-C. Géminard, "Flowers in flour: avalanches in cohesive granular matter," Phys. Rev. E **83**, 051307 (2011).
[47] O. Pouliquen, "Scaling laws in granular flows down rough inclined planes," Phys. Fluids **11**, 542–548 (1999a).
[48] S. Deboeuf, E. Lajeunesse, O. Dauchot, and B. Andreotti, "Flow rule, self-channelization, and levees in unconfined granular flows," Phys. Rev. Lett. **96** (2006).
[49] O. Pitois, P. Moucheront, and X. Chateau, "Liquid bridge between two moving spheres: an experimental study of viscosity effects," J. Colloid Interface Sci. **231**, 26–31 (2000).
[50] X. Chateau, P. Moucheront, and O. Pitois, "Micromechanics of unsaturated granular media," J. Eng. Mech. **128**, 856–863 (2002).
[51] V. Richefeu, M. S. El Youssoufi, R. Peyroux, and F. Radjai, "A model of capillary cohesion for numerical simulations of 3d polydisperse granular media," Int. J. Numerical Anal. Methods Geomech. **32**, 1365–1383 (2008).
[52] H. Rumpf, "Zur theorie der zugfestigkeit von agglomeraten bei kraftuebertragung an kontaktpunkten," Chemie Ing. Technik **42**, 538–540 (1970).
[53] S. Courrech du Pont, P. Gondret, B. Perrin, and M. Rabaud, "Wall effects on granular heap stability," Europhys. Lett. **61**, 492–498 (2003).
[54] R. Mani, D. Kadau, D. Or, and H. J. Herrmann, "Fluid depletion in shear bands," Phys. Rev. Lett. **109**, 248001 (2012).
[55] R. Mani, D. Kadau, and H. J. Herrmann, "Liquid migration in sheared unsaturated granular media," Granular Matter **15**, 447–454 (2013).
[56] J.-Y. Delenne, V. Richefeu, and F. Radjai, "Liquid clustering and capillary pressure in granular media," J. Fluid Mech. **762** (2015).
[57] J.-N. Roux, "A numerical toolkit to understand the mechanics of partially saturated granular materials," J. Fluid Mech. **770**, 1–4 (2015).
[58] A. Gans, O. Pouliquen, and M. Nicolas, "Cohesion-controlled granular material," Phys. Rev. E **101**, 032904 (2020).